



# CHORUS

This is the accepted manuscript made available via CHORUS. The article has been published as:

## Efficient Source of Shaped Single Photons Based on an Integrated Diamond Nanophotonic System

E. N. Knall, C. M. Knaut, R. Bekenstein, D. R. Assumpcao, P. L. Stroganov, W. Gong, Y. Q. Huan, P.-J. Stas, B. Machielse, M. Chalupnik, D. Levonian, A. Suleymanzade, R. Riedinger, H. Park, M. Lončar, M. K. Bhaskar, and M. D. Lukin

Phys. Rev. Lett. **129**, 053603 — Published 26 July 2022

DOI: [10.1103/PhysRevLett.129.053603](https://doi.org/10.1103/PhysRevLett.129.053603)

# Efficient Source of Shaped Single Photons Based on an Integrated Diamond Nanophotonic System

E. N. Knall,<sup>1,\*</sup> C. M. Knaut,<sup>2,\*</sup> R. Bekenstein,<sup>2,3,\*</sup> D. R. Assumpcao,<sup>1,\*</sup> P. L. Stroganov,<sup>2</sup>  
W. Gong,<sup>2</sup> Y. Q. Huan,<sup>2</sup> P. -J. Stas,<sup>2</sup> B. Machielse,<sup>2,4</sup> M. Chalupnik,<sup>2</sup> D. Levonian,<sup>2,4</sup> A.  
Suleymanzade,<sup>2</sup> R. Riedinger,<sup>2,5,6</sup> H. Park,<sup>2,7</sup> M. Lončar,<sup>1</sup> M. K. Bhaskar,<sup>2,4</sup> and M. D. Lukin<sup>2</sup>

<sup>1</sup>*John A. Paulson School of Engineering and Applied Sciences,  
Harvard University, Cambridge, Massachusetts 02138, USA*

<sup>2</sup>*Department of Physics, Harvard University, Cambridge, Massachusetts 02138, USA*

<sup>3</sup>*Racah Institute of Physics, The Hebrew University of Jerusalem, Jerusalem 91904, Israel*

<sup>4</sup>*AWS Center for Quantum Computing, Pasadena, California 91125, USA*

<sup>5</sup>*Institut für Laserphysik und Zentrum für Optische Quantentechnologien, Universität Hamburg, 22761 Hamburg, Germany*

<sup>6</sup>*The Hamburg Centre for Ultrafast Imaging, 22761 Hamburg, Germany*

<sup>7</sup>*Department of Chemistry and Chemical Biology,  
Harvard University, Cambridge, Massachusetts 02138, USA*

(Dated: June 2022)

An efficient, scalable source of shaped single photons that can be directly integrated with optical fiber networks and quantum memories is at the heart of many protocols in quantum information science. We demonstrate a deterministic source of arbitrarily temporally shaped single-photon pulses with high efficiency (detection efficiency = 14.9%) and purity ( $g^{(2)}(0) = 0.0168$ ) and streams of up to 11 consecutively detected single photons using a silicon-vacancy center in a highly directional fiber-integrated diamond nanophotonic cavity. Combined with previously demonstrated spin-photon entangling gates, this system enables on-demand generation of streams of correlated photons such as cluster states and could be used as a resource for robust transmission and processing of quantum information.

Single optical photons play an essential role in quantum information tasks ranging from quantum communication [1] to measurement-based quantum computing [2, 3]. Many protocols in quantum communication use single photons as information carriers between remote locations since photons experience little decoherence while propagating in an optical fiber or free space over long distances. An efficient, scalable source of single photons is therefore extremely useful in quantum information science and technology [4, 5].

The most promising approaches for realizing single-photon sources are based on single atoms, ions [6–8], or artificial atoms [9–11] coupled to optical cavities. The underlying idea is that by promoting an atom to its excited state in a controlled way, only one photon is emitted per excitation cycle. Meanwhile, the encapsulating optical cavity ensures a high probability of photon collection into a well-defined optical mode. Numerous state-of-the-art demonstrations of single-photon sources have utilized solid-state, cavity-integrated self-assembled quantum dots [4, 12–15], which have recently been used in an experiment demonstrating in-fiber single-photon detection efficiencies of above 50% [16].

However, in addition to single photons and linear optical elements, key quantum communication applications such as complex quantum networks will eventually require the use of more advanced components such as quantum memories and quantum repeaters to correct loss errors in communication channels [17, 18] or serve as a

deterministic nonlinearity to enable quantum logic gates between itinerant photons [19, 20]. The necessity of integrating single photons with other components of future quantum networks creates additional requirements that many present-day single-photon sources do not meet: control over the photon frequency, bandwidth, and temporal profile. In particular, leading quantum memory systems have limited bandwidths, often on the MHz scale, which is several orders of magnitude smaller than the bandwidths of typical state-of-the-art single-photon sources [21, 22]. While bandwidth-tailored sources have been realized with neutral-atoms [23], trapped ions [24], and quantum dots [25, 26], such systems with high end-to-end efficiencies, compatibility with scalable device fabrication, and photonic integration have yet to be demonstrated.

In this Letter, we present a versatile, fiber-coupled single-photon source based on a silicon-vacancy center in diamond which features high efficiency, purity, temporal control, integrability, and access to auxiliary spin memory registers. It can also directly interface with existing quantum memories, enabling future compatibility with repeater-based quantum networks as well as protocols for generation of streams of entangled photonic graph states, which are key resources in rapid one-way quantum communication and measurement-based quantum computation protocols [27–32].

Our system consists of a single negatively charged silicon-vacancy center (SiV) in a diamond nanophotonic cavity. The SiV is an inversion-symmetric point defect which features an optically accessible quantum memory that can be embedded in nanofabricated structures

---

\* These authors contributed equally to this work.

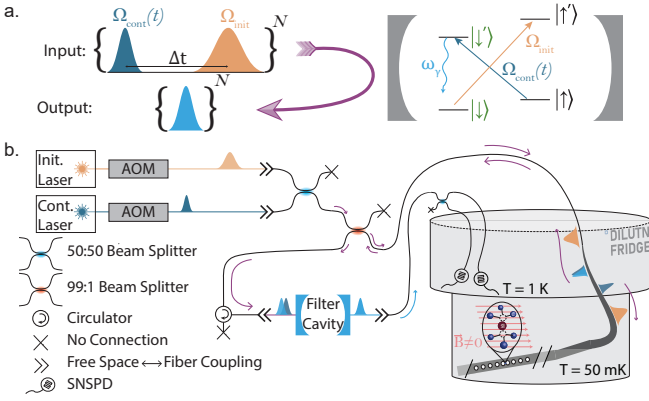


FIG. 1. (a) Photon Creation Schematic. The four-level system of the SiV spin is coherently driven by alternating initializations ( $\Omega_{\text{init}}$ ) and photon generation ( $\Omega_{\text{cont}}$ ) optical pulses, producing a train of temporally shaped photons which are efficiently collected with an overcoupled nanophotonic cavity. (b) Measurement Setup Schematic. A nanophotonic cavity containing an SiV is cooled to 50 mK in a dilution refrigerator and pumped to coherently create single, arbitrarily-shaped photons. Pump pulses are shaped using an acousto-optic modulator, and pump light is filtered out of the single-photon stream by a free space Fabry–Pérot cavity.

while maintaining excellent spin and optical coherence [33, 34]. Our cavity-quantum electrodynamics (CQED) system exhibits strong light-matter coupling, characterized by the single-photon Rabi frequency and cavity and atomic energy decay rates  $\{g, \kappa, \gamma\} = 2\pi \times \{6.81 \text{ GHz}, 329 \text{ GHz}, 0.1 \text{ GHz}\}$ , resulting in a cooperativity of  $C \approx 6$  [35](I.4.2). Unlike in previous experiments where the magnetic field was oriented along the main symmetry axis of the SiV, we apply a magnetic field nearly orthogonal to the SiV’s symmetry axis, giving rise to a four-level system corresponding to the ground ( $|\downarrow\rangle, |\uparrow\rangle$ ) and optically excited ( $|\downarrow'\rangle, |\uparrow'\rangle$ ) states of the SiV’s electronic hole spin [36, 37]. The orthogonal field orientation results in spin-flipping optical transitions becoming allowed, hence enabling fast spin initialization and photon generation [38, 39].

The protocol for single-photon generation in this system is illustrated schematically in Fig. 1a. First, the four-level system is initialized in  $|\uparrow\rangle$  by optically pumping the spin flipping transition  $|\downarrow\rangle \rightarrow |\uparrow\rangle$  using a classical driving field with Rabi frequency  $\Omega_{\text{init}}$ . Then, the population is coherently transferred to a single photon using a control pulse with Rabi frequency  $\Omega_{\text{cont}}$  to drive the transition  $|\uparrow\rangle \rightarrow |\downarrow'\rangle$ . Repeated application of this pulse sequence generates streams of single photons.

The temporal profile of the single-photon wavepackets can be tuned on timescales much longer than the excited state  $|\downarrow'\rangle$  lifetime due to the long-lived quantum memory of the SiV spin. In the limit of weak driving  $|\Omega_{\text{cont}}| \ll \Gamma$ , where  $\Gamma$  is the cavity-enhanced decay rate along  $|\downarrow'\rangle \rightarrow |\downarrow\rangle$ , the dynamics of the excited state  $|\downarrow'\rangle$  adiabatically follows the excitation process [35](II) and

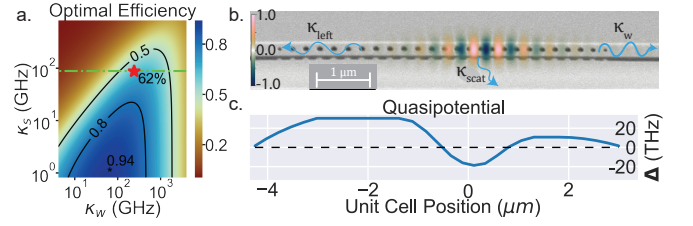


FIG. 2. (a) Photon extraction efficiency is shown in the color plot as a function of cavity-waveguide coupling  $\kappa_w$  and unwanted cavity loss rate  $\kappa_s$ . Contours aid readability of color map. Optimal extraction efficiency is maximized by trading off atom-photon interaction probability, proportional to  $(\kappa_s + \kappa_w)^{-1}$ , for a higher cavity-waveguide coupling rate  $\kappa_w$ . The dashed-dot line cut corresponds to  $\kappa_s = 89 \text{ GHz}$ , the unwanted loss rate of this device, which is determined by fabrication imperfections. The red star highlights this device with waveguide coupling rate  $\kappa_w = 240 \text{ GHz}$ , which is nearly optimal for the given  $\kappa_s$ . (b) A scanning electron micrograph (SEM) of the nanophotonic cavity is overlaid with the simulated electric field, and loss rates are labeled, where  $\kappa_s = \kappa_{\text{scat}} + \kappa_{\text{left}}$ . (c) The simulated quasipotential shape of the cavity [35](I.1) shows that there is a lower and shorter potential barrier on the weak mirror side. This corresponds to the coupling to the right waveguide being the dominant loss rate ( $\kappa_w \gg \kappa_s$ ).

the photon linewidth is limited only by the coherence of the spin-levels  $\{|\downarrow\rangle, |\uparrow\rangle\}$  and the control laser’s linewidth, rather than the intrinsic lifetime of the SiV excited state  $|\downarrow'\rangle$ . By modulating the strength and shape of the control pulse  $\Omega_{\text{cont}}(t)$ , we temporally shape the single photon.

The schematic of our experimental setup is shown in Fig. 1b. Devices are placed in a dilution refrigerator at  $T \approx 50 \text{ mK}$  to reduce the population of phonons which cause thermal mixing between orbital states [38, 40]. This extends the coherence of the ground-state spin, enabling generation of temporally longer photon pulse shapes. Optical control pulses are delivered, and single photons are collected via a tapered optical fiber, which is coupled to the device [41]. On the return path, the generated single photons are filtered from the control pulses by a free space Fabry–Pérot cavity (linewidth = 160 MHz, finesse = 312) before being detected by superconducting nanowire single-photon detectors (SNSPDs).

In order to maximize the photon collection efficiency from the emitter, we implement a novel asymmetric nanophotonic cavity design which strikes a balance between high quality factor of the cavity and strong waveguide damping. In this design, for a given unwanted cavity loss rate  $\kappa_s$  set by fabrication imperfections, there is an optimal choice of waveguide coupling  $\kappa_w$  (Fig. 2a). We achieve this optimal trade-off in the asymmetric diamond nanophotonic cavity as pictured in the scanning electron micrograph (SEM) of Fig. 2b, which preferentially sends light to the coupling waveguide (i.e. to the right side).

These devices are designed using the analogy between a massive particle tunneling through a potential barrier

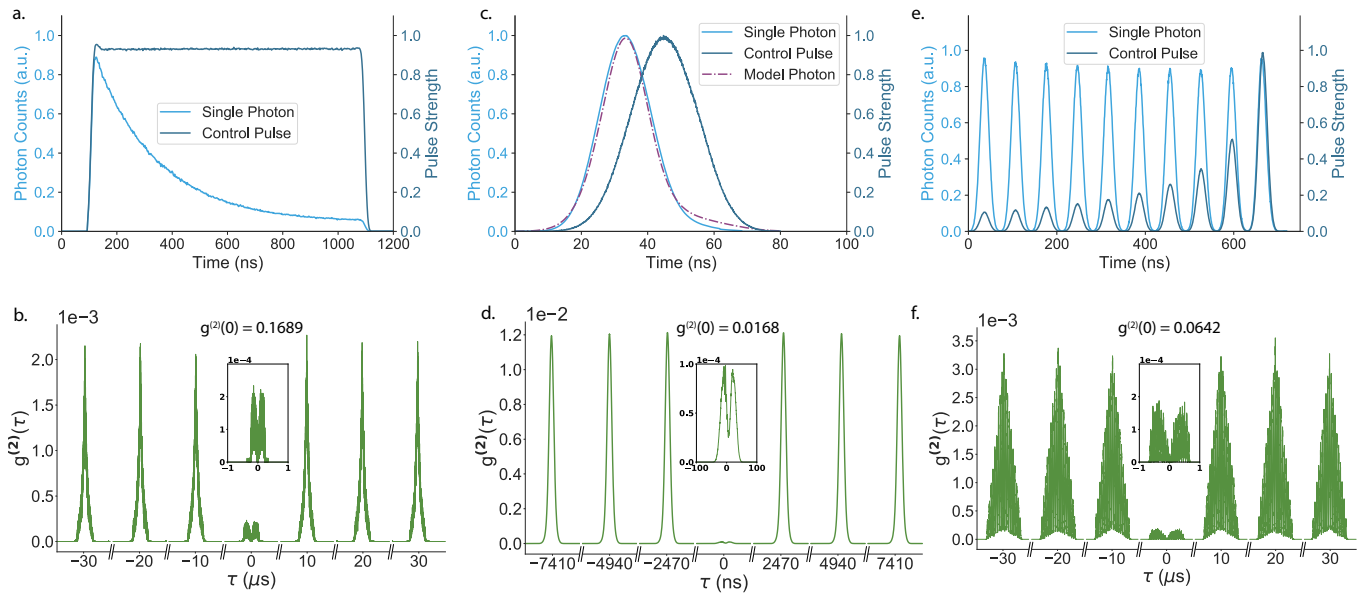


FIG. 3. Pulse-shaped single-photon generation. Upper panels (a), (c), (e) display the temporal profile of the coherent control pulse and detected single photon. (a) A square control pulse produces an exponentially decaying photon. (b) A Gaussian single photon. (c) A single photon distributed over ten time bins (e). Lower panels (b), (d), (f) display the normalized second order correlation of photon arrivals for the exponential, Gaussian, and ten peaked photons respectively. The insets show a zoomed-in window around  $\tau = 0$ , which is integrated to calculate  $g^{(2)}(0)$ .

and the evanescent decay of a photon in a photonic band gap [42]. The asymmetric “quasipotential” for a photon in this device is shown in Fig. 2c. It illustrates both the preferential coupling to the measurement port through the lower and narrower barrier on the right side of the cavity as well as a deep well needed for the tight confinement of the optical mode. The simulated electric field overlay in Fig. 2b illustrates this wavelength scale confinement (mode volume =  $0.67 \left(\frac{\lambda}{n}\right)^3$ ). An in-depth discussion of the new photonic crystal cavity design techniques used here is provided in section I of the Supplementary Information [35].

We demonstrate generation of bandwidth-tailored photons with this platform in Fig. 3. We start by applying a  $1 \mu\text{s}$  square pump pulse (Fig. 3a), and observing an exponentially shaped emitted photon, directly illustrating the optical pumping dynamics from  $|\uparrow\rangle$  into  $|\downarrow\rangle$  expected from a time-independent pump pulse. The photon duration of  $\sim 1 \mu\text{s}$  compared to the  $\sim 1 \text{ ns}$  excited state lifetime highlights the ability of this protocol to generate narrow-bandwidth photons, which is independently verified using a separate narrow filter cavity with linewidth below 5 MHz (Fig 5b). To ensure the presence of only a single photon in each wavepacket, we measure the second order correlation,  $g^{(2)}$ , of the generated photon stream by using a beam splitter and recording the arrival times of photons on a pair of SNSPDs. The results of these measurements are shown in the lower panels of Fig. 3. A value of  $g^{(2)}(0) = 0.1689 < 0.5$  (Fig. 3b) of the exponentially shaped photon confirms the quantum nature of the measured state of light and the presence of a single

excitation.

Next, we apply shorter and more powerful Gaussian control pulses to create Gaussian single photons with full-width half-maxima of  $\sim 20 \text{ ns}$  (Fig. 3c) and observe a substantially reduced  $g^{(2)}(0) = 0.0168$  (Fig. 3d). We note that photons of this approximate duration are optimal for interfacing with existing SiV quantum memories [35, 43].

We confirm our understanding of the system using a density matrix model [35](III) to predict the photon shapes resulting from the applied Gaussian control pulse. Fig. 3c confirms that our model matches the measured photon shape well. By inverting this model, we can calculate the control pulse  $\Omega_{\text{cont}}(t)$  required to generate arbitrarily shaped photon wavepackets. For example, in Fig. 3e, we demonstrate a ten-peaked single photon, which could be useful for time-binned multiplexing [43] and efficient high-dimensional quantum communication [44, 45]. Auto-correlation measurements again demonstrate the single-photon nature of the ten-peaked photon with a low  $g^{(2)}(0) = 0.0642$ . The difference in single-photon purity between the three generated photon shapes can be attributed to optically-induced heating, which results in a reduced spin lifetime and increased value of  $g^{(2)}(0)$  for longer-duration photons [35](VI.2).

Next, we measure the total system efficiency by generating short Gaussian photons (as in Fig. 3c) continuously over a 24 hour period. The repetition rate of the pump pulses is 405 kHz. We record the number of consecutive  $n$ -photon streams detected (Fig. 4) as a proxy for the complexity of multi-photon states that are necessary for

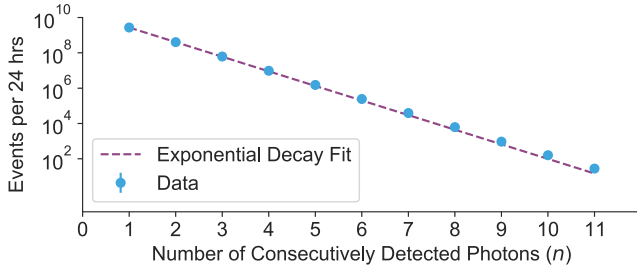


FIG. 4. Statistics of consecutive  $n$ -photon streams detected during a 24-hour acquisition at a 405 kHz repetition rate and 57% average duty cycle, showing detection of up to 11 photons in a row. Exponential decay fit indicates a total source-to-detector efficiency of 14.9%.

implementation of quantum information protocols such as one-way quantum communication or computing with photonic cluster states [27–32]. Notably, the experiment was operating autonomously during this 24-hour run. Our experiment control software [46] automatically handles SiV ionization and spectral diffusion events, as well as filter cavity locking [35](IV.2), making this a realistic demonstration of a practical single-photon source.

The exponential decay fit to the  $n$ -photon event rates reveals a single-photon detection efficiency of 14.9% [35](V.1). This decrease compared to the ideal photon extraction efficiency of 62% is primarily due to losses in the filtering setup (0.5-0.6), waveguide-fiber coupling efficiency (0.7), and finite detuning of the cavity [35](IV.3). Despite these extra losses, this single-photon efficiency is competitive with state-of-the-art single-photon sources [4, 12, 47]. A single-photon detection rate of 31 kHz is achieved, indicating an average duty cycle of 57%, which is primarily limited by ionization of the SiV and software overhead [35](V.2).

As a first step toward generation of spin-photon entangled states and more complex multi-photon entangled states, we next explore the light-matter interface with the auxiliary nuclear spin memory associated with the  $^{29}\text{Si}$  isotope. The hyperfine coupling between the electronic hole spin and the nuclear spin additionally splits the electronic-hole Zeeman ground state manifold creating four levels in the ground-state manifold (Fig. 5a). As a result, the  $^{29}\text{SiV}$  system can emit photons with two nuclear spin dependent photon frequencies,  $\nu_{\uparrow}$  and  $\nu_{\downarrow}$ . Such a system can be used to generate complex multi-photon entangled states such as cluster states or graph states, as proposed in [30, 32], by coherently manipulating the nuclear state in between emissions of subsequent photons.

In order to probe the nuclear spin dependent emission frequency of a cavity-integrated  $^{29}\text{SiV}$ , we filter the single-photon signal using a significantly narrower 5 MHz linewidth filter cavity, locked close to the  $|\downarrow'\rangle \rightarrow |\downarrow\rangle$  transition. The photons are generated via the same scheme as before, whereby a single initialization pulse is used to

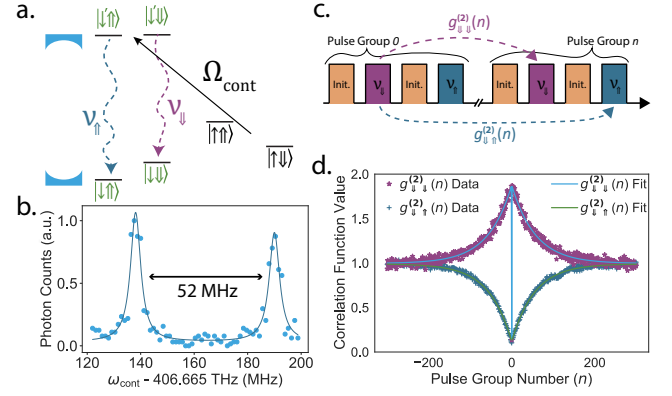


FIG. 5. Hyperfine splitting due to the  $^{29}\text{Si}$  nuclear spin (a) gives rise to a four-level ground state manifold. Pumping on the electron-spin flipping transition with  $\Omega_{\text{cont}}$  results in the generation of photons with two nuclear-state dependent frequencies  $\nu_{\uparrow}$  and  $\nu_{\downarrow}$ . (b) Sweeping the control pulse frequency selectively tunes  $\nu_{\uparrow}$  and  $\nu_{\downarrow}$  into resonance with the filter cavity, which enables the measurement of the spectrum of the emitted photons. (c) Pulse sequence for attempting to measure either two consecutive photons at nuclear-state dependent frequencies  $\nu_{\downarrow}$  and  $\nu_{\downarrow}$  or at nuclear-state dependent frequencies  $\nu_{\downarrow}$  and  $\nu_{\uparrow}$ . (d) (Purple)  $g_{\downarrow\downarrow}^{(2)}(\tau)$  auto-correlation measurements of the photons emitted at  $\nu_{\downarrow}$  show antibunching at zero time delay, and bunching after emission of  $113.8 \pm 3.8$  photons (1.48 ms timescale). (Blue)  $g_{\downarrow\uparrow}^{(2)}(\tau)$  cross-correlation function for the two consecutively emitted photons at  $\nu_{\uparrow}$  and  $\nu_{\downarrow}$  shows anti-bunching after emission of  $110.6 \pm 2.4$  photons, suggesting that the nuclear polarization is preserved for repeated generation of up to 110 photons.

initialize the electron regardless of the initial nuclear spin state due to the small hyperfine splitting as compared to the optical transition bandwidth. The filter cavity frequency is held constant while the frequency of the pump laser is swept tuning the frequency of the emitted photons. This selectively tunes  $\nu_{\uparrow}$  and  $\nu_{\downarrow}$  into resonance with the filter cavity, enabling the measurement of the spectrum of the emitted photons. Two narrow peaks are observed in the detected single-photon spectrum with a splitting of 52 MHz (Fig. 5b), as expected from the hyperfine splitting from the  $^{29}\text{Si}$  nuclear spin [48].

An initial step toward generating multi-photon states with entanglement mediated by the  $^{29}\text{SiV}$  nuclear spin is to show that multiple photons can be generated while preserving the nuclear spin state. Therefore, we measure correlations between subsequently emitted photons at the two different nuclear spin dependent emission frequencies,  $\nu_{\uparrow}$  and  $\nu_{\downarrow}$  (Fig. 5c). We measure the degree of second-order correlations  $g_{\downarrow\downarrow}^{(2)}(\tau)$  of photons emitted at frequency  $\nu_{\downarrow}$ , observing bunching on long timescales. We then measure the intensity cross-correlation  $g_{\downarrow\uparrow}^{(2)}(\tau) = \langle I_{\downarrow}(t)I_{\uparrow}(t+\tau) \rangle / \langle I_{\downarrow}(t)I_{\uparrow}(t) \rangle$ , where  $I_{\uparrow}$  and  $I_{\downarrow}$  are the intensities of the  $\nu_{\uparrow}$  and  $\nu_{\downarrow}$  emissions, respectively, and observe anti-bunching on the same timescale. These measurements indicate a 16-fold higher probability of detect-

ing subsequently emitted photons at the same frequency, as opposed to opposite frequencies.

The bunching (antibunching) in  $g_{\downarrow\downarrow}^{(2)}(\tau)$  ( $g_{\downarrow\uparrow}^{(2)}(\tau)$ ) decays after emission of  $113.8 \pm 3.8$  ( $110.6 \pm 2.4$ ) photons. We attribute this decay to relaxation of the nucleus due to the single-photon generation process. Relaxation of the nucleus after emission of  $113.8 \pm 3.8$  photons would correspond to each generated photon inducing a nuclear spin flip with a probability of  $(0.9 \pm 0.03)\%$ . These measurements directly demonstrate that classical correlations between the  $^{29}\text{Si}$  nuclear spin state and the frequency of the emitted photon can persist for more than 100 consecutively emitted photons, making this a promising approach for the generation of large-scale photonic graph states [32].

Our experiments demonstrate an on-demand source of streams of shaped photons generated from a silicon-vacancy center in an asymmetric nanophotonic cavity in diamond. The challenge of producing a nanophotonic cavity in diamond with arbitrary coupling ratios was resolved through the development of a quasipotential design heuristic, which we believe will be of general use to the nanophotonics community. We showed that the system can generate single photons with highly tunable temporal wavepackets and high spectral purity, detecting streams of up to 11 sequential photons at experimentally useful rates due to a high source-to-detector efficiency and efficient fiber-nanophotonic integration. Given the measured  $g^{(2)}(0) = 0.0168$ , we estimate this source would provide more than a thirty-fold improvement in the single-photon detection rate when used as a replacement for a weak coherent source with equivalent two-photon detection infidelity [35](V.3). Furthermore, this advantage results in an exponential improvement for higher  $n$ -photon stream events, as demonstrated by the detection of 28 total 11-photon events in a 24 hour period, which is comparable to state-of-the-art [49].

Additionally, this single-photon source should enable the generation of multi-photon entangled states when efficiently interfaced with a second cavity-coupled SiV [43], which would be used as a quantum memory to deterministically entangle subsequent photons [32]. By demonstrating classical correlations between the built-in  $^{29}\text{Si}$  nuclear spin state and emitted photon frequency, we also illustrate the possibility to directly generate streams of entangled photons mediated by nuclear memory. In order to demonstrate quantum correlations (i.e. entanglement) between nuclear spin and photon frequency, additional coherent control of the nucleus would be necessary, which should be possible using RF fields supplied by on-chip coplanar waveguides [33, 34]. Moreover, in order to realize large entangled states, mitigation of  $^{29}\text{Si}$  memory decoherence arising from heating, which shortens the electron lifetime, will be required [35](VI.1).

This work builds on our previous demonstration of the SiV-based quantum memory node [43]. The photons generated by our source can be bandwidth and wavelength

matched to existing SiV-nanophotonic quantum memory devices, which will be required for complex quantum networking schemes involving stationary repeaters or quantum memories. Combined with the demonstrated ability to create large multi-photon streams on demand, this method should enable the production and detection of high photon number linear cluster states with only moderate improvements to the setups demonstrated here and in [35, 43]. For these reasons, our platform demonstrates promise as a versatile single-photon source which can be interfaced with quantum memories for the realization of quantum networking and quantum information processing tasks.

The authors thank Denis Sukachev and Yan-Cheng Wei for their insightful discussions and feedback on the manuscript, as well as Jim MacArthur for assistance with electronics. This work was supported by the NSF (PHY-2012023), NSF EFRI ACQUIRE (5710004174), CUA (PHY-1734011), DoE (DE-SC0020115), AFOSR MURI (FA9550171002 and FA95501610323), and CQN (EEC-1941583). Devices were fabricated in the Harvard University Center for Nanoscale Systems (CNS), a member of the National Nanotechnology Coordinated Infrastructure Network (NNCI), which is supported by the National Science Foundation under NSF award no. 1541959. ENK, DA, and BM acknowledge that this material is based upon work supported by the National Science Foundation Graduate Research Fellowship under Grant No. DGE1745303. YQH acknowledges support from the Agency for Science, Technology and Research (A\*STAR) Singapore through the National Science Scholarship. MC and MKB acknowledge support from the Department of Defense (DoD) through the National Defense Science and Engineering Graduate (NDSEG) Fellowship Program. RR acknowledges support from the Alexander von Humboldt Foundation and the Cluster of Excellence ‘Advanced Imaging of Matter’ of the Deutsche Forschungsgemeinschaft (DFG) - EXC 2056 - project ID 390715994. The color maps used in Fig. 2 were designed by [50].

- 
- [1] H. J. Kimble, *Nature* **208** 453:7198 **453**, 1023 (2008).
  - [2] R. Raussendorf and H. J. Briegel, *Physical Review Letters* **86**, 5188 (2001).
  - [3] P. Kok, W. J. Munro, K. Nemoto, T. C. Ralph, J. P. Dowling, and G. J. Milburn, *Reviews of Modern Physics* **79**, 135 (2007).
  - [4] H. Wang, Y. M. He, T. H. Chung, H. Hu, Y. Yu, S. Chen, X. Ding, M. C. Chen, J. Qin, X. Yang, R. Z. Liu, Z. C. Duan, J. P. Li, S. Gerhardt, K. Winkler, J. Jurkat, L. J. Wang, N. Gregersen, Y. H. Huo, Q. Dai, S. Yu, S. Höfling, C. Y. Lu, and J.-W. Pan, *Nature Photonics* **13**, 770 (2019).
  - [5] M. D. Eisaman, J. Fan, A. Migdall, and S. V. Polyakov, *Review of Scientific Instruments* **82**, 071101 (2011).
  - [6] A. Kuhn, M. Hennrich, and G. Rempe, *Physical Review*

- Letters **89**, 4 (2002).
- [7] J. McKeever, A. Boca, A. D. Boozer, R. Miller, J. R. Buck, A. Kuzmich, and H. J. Kimble, *Science* **303**, 1992 (2004).
- [8] M. Keller, B. Lange, K. Hayasaka, W. Lange, and H. Walther, *Nature* **431**:7012 **431**, 1075 (2004), very early trapped ion CQED based SPS.
- [9] P. Michler, A. Imamoglu, M. D. Mason, P. J. Carson, G. F. Strouse, and S. K. Buratto, *Nature* **406**:6799 **406**, 968 (2000).
- [10] Z. Yuan, B. E. Kardynal, R. M. Stevenson, A. J. Shields, C. J. Lobo, K. Cooper, N. S. Beattie, M. Pepper, and M. Pepper, *Science* **295**, 102 (2002).
- [11] A. Beveratos, R. Brouri, T. Gacoin, A. Villing, J.-P. Poizat, and P. Grangier, *Physical Review Letters* **89**, 187901 (2002).
- [12] R. Uppu, F. T. Pedersen, Y. Wang, C. T. Olesen, C. Papon, X. Zhou, L. Midolo, S. Scholz, A. D. Wieck, A. Ludwig, and P. Lodahl, *Science Advances* **6**, 1 (2020).
- [13] Y.-M. He, J. Liu, S. Maier, M. Emmerling, S. Gerhardt, M. Davanço, K. Srinivasan, C. Schneider, and S. Höfling, *Optica* **4**, 802 (2017).
- [14] S. Unsleber, Y.-M. He, S. Gerhardt, S. Maier, C.-Y. Lu, J.-W. Pan, N. Gregersen, M. Kamp, C. Schneider, and S. Höfling, *Optics Express* **24**, 8539 (2016).
- [15] M. Arcari, I. Söllner, A. Javadi, S. L. Hansen, S. Mahmoodian, J. Liu, H. Thyrrerstrup, E. Lee, J. Song, S. Stobbe, and P. Lodahl, *Physical Review Letters* **113**, 093603 (2014).
- [16] N. Tomm, A. Javadi, N. O. Antoniadis, D. Najer, M. C. Löbl, A. R. Korsch, R. Schott, S. R. Valentin, A. D. Wieck, A. Ludwig, and R. J. Warburton, *Nature Nanotechnology* **16**, 399 (2021).
- [17] H. J. Briegel, W. Dür, J. I. Cirac, and P. Zoller, *Physical Review Letters* **81**, 5932 (1998).
- [18] S. Muralidharan, J. Kim, N. Lütkenhaus, M. D. Lukin, and L. Jiang, *Physical Review Letters* **112**, 1 (2014).
- [19] N. Kalb, A. Reiserer, S. Ritter, and G. Rempe, *Physical Review Letters* **114**, 220501 (2015).
- [20] L. M. Duan and H. J. Kimble, *Physical Review Letters* **92**, 1 (2004).
- [21] B. Baek, M. J. Stevens, S. W. Nam, and S. D. Dyer, *Optics Express*, Vol. 16, Issue 13, pp. 9966-9977 **16**, 9966 (2008).
- [22] X. song Ma, S. Zotter, J. Kofler, T. Jennewein, and A. Zeilinger, *Physical Review A* **83**, 043814 (2011).
- [23] M. Mücke, J. Bochmann, C. Hahn, A. Neuzner, C. Nölleke, A. Reiserer, G. Rempe, and S. Ritter, *Physical Review A* **87**, 1 (2013).
- [24] J. Schupp, V. Krcmarsky, V. Krutyanskiy, M. Meraner, T. Northup, and B. Lanyon, *PRX Quantum* **2**, 1 (2021).
- [25] B. C. Pursley, S. G. Carter, M. K. Yakes, A. S. Bracker, and D. Gammon, *Nature Communications* **2017** 9:1 **9**, 1 (2018).
- [26] Y. He, Y.-M. He, Y.-J. Wei, X. Jiang, M.-C. Chen, F.-L. Xiong, Y. Zhao, C. Schneider, M. Kamp, S. Höfling, C.-Y. Lu, and J.-W. Pan, *Physical Review Letters* **111**, 237403 (2013).
- [27] J. Borregaard, H. Pichler, T. Schröder, M. D. Lukin, P. Lodahl, and A. S. Sørensen, *Physical Review X* **10**, 21071 (2020).
- [28] I. Schwartz, D. Cogan, E. R. Schmidgall, Y. Don, L. Gantz, O. Kenneth, N. H. Lindner, and D. Gershoni, *Science* **354**, 434 (2016).
- [29] M. Gimeno-Segovia, T. Rudolph, and S. E. Economou, *Physical Review Letters* **123**, 070501 (2019).
- [30] K. Tiurev, M. H. Appel, P. L. Mirambell, M. B. Lauritzen, A. Tiranov, P. Lodahl, and A. S. Sørensen, *Phys. Rev. A* **105**, L030601 (2022).
- [31] D. Buterakos, E. Barnes, and S. E. Economou, *Physical Review X* **7**, 041023 (2017).
- [32] N. H. Lindner and T. Rudolph, *Physical Review Letters* **103**, 113602 (2009).
- [33] C. T. Nguyen, D. D. Sukachev, M. K. Bhaskar, B. Machielse, D. S. Levonian, E. N. Knall, P. Stroganov, R. Riedinger, H. Park, M. Lončar, and M. D. Lukin, *Physical Review Letters* **123**, 1 (2019).
- [34] C. T. Nguyen, D. D. Sukachev, M. K. Bhaskar, B. Machielse, D. S. Levonian, E. N. Knall, P. Stroganov, C. Chia, M. J. Burek, R. Riedinger, H. Park, M. Lončar, and M. D. Lukin, *Physical Review B* **100**, 1 (2019).
- [35] See Supplementary Material for further clarification and discussion. Supplement includes Refs. [51-64].
- [36] C. Hepp, PhD Dissertation, Universität des Saarlandes [10.22028/D291-23020](https://doi.org/10.22028/D291-23020) (2014).
- [37] C. Hepp, T. Müller, V. Waselowski, J. N. Becker, B. Pingault, H. Sternschulte, D. Steinmüller-Nethl, A. Gali, J. R. Maze, M. Atatüre, and C. Becher, *Physical Review Letters* **112**, 1 (2014).
- [38] D. Sukachev, A. Sipahigil, C. Nguyen, M. Bhaskar, R. Evans, F. Jelezko, and M. Lukin, *Physical Review Letters* **119**, 223602 (2017).
- [39] L. J. Rogers, K. D. Jahnke, M. H. Metsch, A. Sipahigil, J. M. Binder, T. Teraji, H. Sumiya, J. Isoya, M. D. Lukin, P. Hemmer, and F. Jelezko, *Physical Review Letters* **113**, 263602 (2014).
- [40] K. D. Jahnke, A. Sipahigil, J. M. Binder, M. W. Doherty, M. Metsch, L. J. Rogers, N. B. Manson, M. D. Lukin, and F. Jelezko, *New Journal of Physics* **17**, 043011 (2015).
- [41] M. J. Burek, C. Meuwly, R. E. Evans, M. K. Bhaskar, A. Sipahigil, S. Meesala, B. Machielse, D. D. Sukachev, C. T. Nguyen, J. L. Pacheco, E. Bielejec, M. D. Lukin, and M. Lončar, *Physical Review Applied* **8**, 024026 (2017).
- [42] J. D. Joannopoulos, S. G. Johnson, J. N. Winn, and R. D. Meade, *Photonic Crystals: Molding the Flow of Light (Second Edition)* (2008).
- [43] M. K. Bhaskar, R. Riedinger, B. Machielse, D. S. Levonian, C. T. Nguyen, E. N. Knall, H. Park, D. Englund, M. Lončar, D. D. Sukachev, and M. D. Lukin, *Nature* **580**, 60 (2020).
- [44] J. Miguel-Ramiro and W. Dür, *Physical Review A* **98**, 042309 (2018).
- [45] D. Cozzolino, B. D. Lio, D. Bacco, and L. K. Oxenløwe, *Advanced Quantum Technologies* **2**, 1900038 (2019).
- [46] C. M. Knaut, M. Bhaskar, P. Stroganov, Y. Q. Huan, P.-J. Stas, D. Assumpcao, and W. Gong, *pylabnet - Client-server, python-based laboratory software* (2021).
- [47] G. Kiršanske, H. Thyrrerstrup, R. S. Daveau, C. L. Dreeßen, T. Pregolato, L. Midolo, P. Tighineanu, A. Javadi, S. Stobbe, R. Schott, A. Ludwig, A. D. Wieck, S. I. Park, J. D. Song, A. V. Kuhlmann, I. Söllner, M. C. Löbl, R. J. Warburton, and P. Lodahl, *Physical Review B* **96**, 1 (2017).
- [48] B. Pingault, D.-D. Jarausch, C. Hepp, L. Klintberg, J. N. Becker, M. Markham, C. Becher, and M. Atatüre, *Nature Communications* **2017** 8:1 **8**, 1 (2017).
- [49] H.-S. Zhong, Y. Li, W. Li, L.-C. Peng, Z.-E. Su, Y. Hu, Y.-M. He, X. Ding, W. Zhang, H. Li, L. Zhang, Z. Wang, L. You, X.-L. Wang, X. Jiang, L. Li, Y.-A. Chen, N.-L.

- Liu, C.-Y. Lu, and J.-W. Pan, *Physical Review Letters* **121**, 250505 (2018).
- [50] F. Cramer, G. E. Shephard, and P. J. Heron, *Nature Communications* **11**, 1 (2020).
- [51] P. Lodahl, S. Mahmoodian, and S. Stobbe, *Rev. Mod. Phys.* **87**, 347 (2015).
- [52] M. Lobet, I. Liberal, E. N. Knall, M. Z. Alam, O. Reshef, R. W. Boyd, N. Engheta, and E. Mazur, *ACS Photonics* **7**, 1965 (2020).
- [53] Q. Quan, P. B. Deotare, and M. Lončar, *Applied Physics Letters* **96**, 17 (2010).
- [54] R. E. Evans, M. K. Bhaskar, D. D. Sukachev, C. T. Nguyen, A. Sipahigil, M. J. Burek, B. Machielse, G. H. Zhang, A. S. Zibrov, E. Bielejec, H. Park, M. Lončar, and M. D. Lukin, *Science* **362**, 662 (2018).
- [55] M. J. Kastoryano, F. Reiter, and A. S. Sørensen, *Physical Review Letters* **106**, 2 (2011).
- [56] J. Borregaard, P. Kómár, E. M. Kessler, M. D. Lukin, and A. S. Sørensen, *Physical Review A* **92**, 1 (2015).
- [57] A. Reiserer and G. Rempe, *Rev. Mod. Phys.* **87**, 1379 (2015).
- [58] T. G. Tiecke, J. D. Thompson, N. P. De Leon, L. R. Liu, V. Vuletić, and M. D. Lukin, *Nature* **508**, 241 (2014).
- [59] V. Weisskopf and E. Wigner, in *Part I: Particles and Fields. Part II: Foundations of Quantum Mechanics* (Springer, 1997) pp. 30–49.
- [60] J. Johansson, P. Nation, and F. Nori, *Computer Physics Communications* **184**, 1234 (2013).
- [61] P. Senellart, G. Solomon, and A. White, *Nature Nanotechnology* **2017 12:11** **12**, 1026 (2017).
- [62] S. Meesala, Y.-I. Sohn, B. Pingault, L. Shao, H. A. Atikian, J. Holzgrafe, M. Gündoğan, C. Stavrakas, A. Sipahigil, C. Chia, R. Evans, M. J. Burek, M. Zhang, L. Wu, J. L. Pacheco, J. Abraham, E. Bielejec, M. D. Lukin, M. Atatüre, and M. Lončar, *Phys. Rev. B* **97**, 205444 (2018).
- [63] B. Machielse, S. Bogdanovic, S. Meesala, S. Gauthier, M. Burek, G. Joe, M. Chalupnik, Y. Sohn, J. Holzgrafe, R. Evans, C. Chia, H. Atikian, M. Bhaskar, D. Sukachev, L. Shao, S. Maity, M. Lukin, and M. Lončar, *Physical Review X* **9**, 031022 (2019).
- [64] Y. Akahane, T. Asano, B. S. Song, and S. Noda, *Nature* **425**, 944 (2003).